Science AAAS

Manuscript submitted for publication: Confidential 26 Sept. 2013

Title: Chelyabinsk Airburst, Damage Assessment, Meteorite Recovery and Characterization

Authors: Olga P. Popova[1], Peter Jenniskens[2,3,*], Vacheslav Emel'yanenko[4], Anna Kartashova[4], Eugeny Biryukov[5], Sergey Khaibrakhmanov[6], Valery Shuvalov[1], Yurij Rybnov[1], Alexandr Dudorov[6], Victor I. Grokhovsky[7], Dmitry D. Badyukov[8], Qing-Zhu Yin[9], Peter S. Gural[2], Jim Albers[2], Mikael Granvik[10], Läslo G. Evers[11,12], Jacob Kuiper[11], Vladimir Kharlamov[1], Andrey Solovyov[13], Yuri S. Rusakov[14], Stanislav Korotkiy[15], Ilya Serdyuk[16], Alexander V. Korochantsev[8], Michail Yu. Larionov[7], Dmitry Glazachev[1], Alexander E. Mayer[6], Galen Gisler[17], Sergei V. Gladkovsky[18], Josh Wimpenny[9], Matthew E. Sanborn[9], Akane Yamakawa[9], Kenneth L. Verosub[9], Douglas J. Rowland[19], Sarah Roeske[9], Nicholas W. Botto[9], Jon M. Friedrich[20,21], Michael Zolensky[22], Loan Le[23,22], Daniel Ross[23,22], Karen Ziegler[24], Tomoki Nakamura[25], Insu Ahn[25], Jong Ik Lee[26], Qin Zhou[27, 28], Xian-Hua Li[28], Qiu-Li Li[28], Yu Liu[28], Guo-Qiang Tang[28], Takahiro Hiroi[29], Derek Sears[3], Ilya A. Weinstein[7], Alexander S. Vokhmintsev[7], Alexei V. Ishchenko[7], Phillipe Schmitt-Kopplin[30,31], Norbert Hertkorn[30], Keisuke Nagao[32], Makiko K. Haba[32], Mutsumi Komatsu[33], and Takashi Mikouchi[34] (The Chelyabinsk Airburst Consortium).

Affiliations:

[1] Institute for Dynamics of Geospheres of the Russian Academy of Sciences, Leninsky Prospect 38, Bldg. 1, Moscow, 119334, Russia.

[2] SETI Institute, 189 Bernardo Ave, Mountain View, CA 94043, USA.

[3] NASA Ames Research Center, Moffett Field, Mail Stop 245-1, CA 94035, USA.

[4] Institute of Astronomy of the Russian Academy of Sciences, Pyatnitskaya 48, Moscow, 119017, Russia.

[5] Deptartment of Theoretical Mechanics, South Ural State University, Lenin Avenue 76, Chelyabinsk, 454080, Russia.

[6] Chelyabinsk State University, Bratyev Kashirinyh Street 129, Chelyabinsk, 454001, Russia.

[7] Institute of Physics and Technology, Ural Federal University, Mira Street 19, Yekaterinburg, 620002, Russia.

[8] Vernadsky Institute of Geochemistry and Analytical Chemistry of the RAS, Kosygina Street 19, Moscow, 119991, Russia.

[9] Deptartment of Earth and Planetary Sciences, University of California at Davis, Davis, CA 95616, USA.

[10] Department of Physics, University of Helsinki, P. O. Box 64, 00014 Helsinki, Finland.

[11] Koninklijk Nederlands Meteorologisch Instituut, P. O. Box 201, 3730 AE De Bilt, the Netherlands.

[12] Department of Geoscience and Engineering, Faculty of Civil Engineering and Geosciences, Delft University of Technology, PO Box 5048, 2600 GA Delft, the Netherlands

[13] Tomsk State University, Lenina Propsect 36, Tomsk, 634050 Russia.

[14] Research and Production Association "Typhoon", fl. 2, 7 Engels Street, Obninsk, 249032, Russia.

[15] Support Foundation for Astronomy "Ka-Dar", P.O. Box 82, Razvilka, 142717 Russia.

[16] Science and Technology Center of the Social and Youth Initiatives Organization, 3-12-63 Udal'tsova Street, Moscow, 119415, Russia.

[17] University of Oslo, Physics Building, Sem Saelands Vel 24, 0316 Oslo, Norway.

[18] Institute of Engineering Sciences Urals Branch of the Russian Academy of Sciences, Komsomolskaya Street 34, Yekaterinburg, 620049, Russia.

[19] Center for Molecular and Genomic Imaging, University of California, Davis, Davis, CA 95616, USA.

[20] Department of Earth & Planetary Sciences, American Museum of Natural History, New York, NY 10024, USA.

[21] Department of Chemistry, Fordham University, Bronx, NY 10458, USA.

[22] Astromaterials Research and Exploration Science, NASA Johnson Space Center, Houston, TX 77058, USA.

[23] Jacobs Technology, 2224 Bay Area Blvd., Houston TX 77058, USA.

[24] Institute of Meteoritics, University of New Mexico, Albuquerque, NM 87131-0001, USA.

[25] Department of Earth and Planetary Materials Science, Tohoku University, Aramaki, Aoba, Sendai, Miyagi 980-8578, Japan.

[26] Division of Polar Earth-System Sciences, Korea Polar Research Institute, 26 Songdomi rae, Yeonsu-gu, Incheon 406-840, Korea.

[27] National Astronomical Observatories, Beijing, Chinese Academy of Sciences, Beijing 100012, China.

[28] State Key Laboratory of Lithospheric Evolution, Institute of Geology and Geophysics, Chinese Academy of Sciences, Beijing 100029, China.

[29] Deptartment of Geological Sciences, Brown University, Providence, RI 02912, USA.

[30] Analytical BioGeoChemistry, Helmoltz Zentrum Muenchen, Ingoldstäter Landstrasse 1, D-85764 Obeschleissheim, Germany.

[31] Technical University Muenchen, Analytical Food Chemistry, Alte Akademie 10, 85354 Freising, Germany.

[32] Geochemical Research Center, The University of Tokyo, 7-3-1 Hongo, Bunkyo-ku, Tokyo 113-0033, Japan.

[33] Waseda Institute for Advanced Study, Waseda University, 1-6-1 Nishiwaseda, Shinjuku, Tokyo 169-8050, Japan.

[34] Department of Earth and Planetary Science, The University of Tokyo, 7-3-1 Hongo, Bunkyo-ku, Tokyo 113-0033, Japan.

*To whom correspondence should be addressed. Email: Petrus.M.Jenniskens@nasa.gov

The asteroid impact near the Russian city of Chelyabinsk on February 15th, 2013 was the largest airburst on Earth since the 1908 Tunguska event, causing a natural disaster in an area with a population exceeding one million. Because it occurred in an era with modern consumer electronics, field sensors, and laboratory techniques, unprecedented measurements were made of the impact event and the meteoroid that caused it. Here we document the account of what happened, as understood now, using comprehensive data obtained from astronomy, planetary science, geophysics, meteoritics, and cosmochemistry, and from social science surveys. A good understanding of the Chelyabinsk incident provides a unique opportunity to calibrate the event, with important implications for the future study of near-Earth objects and developing hazard mitigation strategies for planetary protection.

Chelyabinsk Oblast experienced an impact that was 100 times more energetic than the recent 4 kT of TNT equivalent Sutter's Mill (*1*). This was the biggest impact over land since the poorly observed Tunguska in 1908, for which kinetic energy estimates range from 3-5 (*2*) to 10-50 MT (*3*). From the period of infrasound waves circum traveling the globe (*4*), an early estimate of ~ 470 kT was derived for Chelyabinsk (*5*). Infrasound data from Russia and Kazakhstan provide 570±150 kT - see supplementary online material (SOM) Section 1.4 (*6*). Spaceborne visible and near-infrared observations (*7*) recorded a total irradiated energy of 90 kT (*5,8*), corresponding to a kinetic energy of 590±50 kT using the calibration by Nemtchinov *et al.* (*9*). All values are uncertain by a factor of two because of lack of calibration data at those high energies and altitudes.

The manner in which this kinetic energy was deposited in the atmosphere determined what shock wave reached the ground. Dash-cam and security camera videos of the fireball (Fig. 1) provide a lightcurve with peak brightness of -27.3±0.5 magnitude (Fig. 2; SOM Sect. 1.2). The integrated lightcurve is consistent with other energy estimates if the panchromatic luminous efficiency was 7±3 %. Theoretical estimates under these conditions range from 5.6 - 13.2% (*10*).

Calibrated video observations provided a trajectory and pre-atmospheric orbit (Table 1; SOM Sect. 1.1). The fireball was first recorded at 97 km altitude, moving at 19.16±0.15 km/s and entry angle 18.3±0.2º with the horizontal, which is slightly faster than reported earlier (*11*). Combined with the best kinetic energy estimate, an entry mass of 1.3×10^7 kg (with factor two uncertainty) and a diameter of 19.8±4.6 m is derived, assuming a spherical shape and the meteorite-derived density of 3.3 g/cm^3 based on X-ray computed tomography (SOM Sect. 4.2, Table S16).

Size and speed suggest that a shock wave first developed at 90 km. Observations show that dust formation and fragmentation started around 83 km and accelerated at 54 km (Fig. S16, S22). Peak radiation occurred at 29.7±0.7 km altitude at 03:20:32.2±0.1s UTC (SOM Sect. 1.1-2), at which time spaceborne sensors measured a meteoroid speed of 18.6 km/s (*5*). Fragmentation left a thermally emitting debris cloud in this period leading to a burst at 27.0 km that settled to 26.2 km (Fig. 1), resulting in a distinctly higher billowing above that location (Fig. S22). The dust cloud split in two due to buoyancy of the hot gas, leading to two cylindrical vortices (*12*).

Compared to Tunguska (*2,3*), Chelyabinsk was on the threshold of forming a common shock wave around the fragments when it broke at peak brightness (SOM Sect. 1.2). Fragments were

enough spatially isolated enough to be efficiently decelerated, avoiding the transfer of momentum to lower altitudes and more damage when the blast wave reached the ground.

Damage Assessment

In the weeks following the event, 50 villages were visited to verify the extent of glass damage. The resulting map (Fig. 3) demonstrates that the shockwave had a cylindrical component, extending furthest perpendicular to the trajectory. There was little coherence of the shockwave in forward direction, where the perturbance was of long duration, shaking buildings and making people run outside, but causing no damage.

The strength of this shockwave on the ground was modeled (SOM Sect. 2.4) assuming that an overpressure of $\Delta P > 500$ Pa is required (13). A 540 kT event, with detonations spread over altitudes 34-27 km and around 24-19 km, would cause damage out to 108 km distance with the correct shape (Fig. 3). The fragments penetrating below 27 km must have contributed to the damage in order to match the shock wave arrival times (SOM Sect. 2.4). The number of houses damaged per 1,000 inhabitants (Table S11, SOM Sect. 2.3) falls off with distance from the airburst source (r) as $r^{-2.6\pm1.2}$, with overpressure calculated to fall off as $r^{-2.4}$ (Fig. S39). In Chelyabinsk itself, 3,613 apartment buildings (about 44%) had shattered and broken glass, but these were not evenly distributed in the city (Fig. S37). Sharp sounds heard following the shockwave also point to the fragmentation causing a complicated distribution of pressure. Structural damage included the collapse of a zinc factory roof.

Directly below the fireball's path, the shock wave was strong enough to blow people off their feet. In Yemanzhelinsk, window frames facing the trajectory were pushed inwards, and suspended ceilings were sucked down above broken windows (Fig. S36G). There was no structural damage, other than a statue of Pushkin inside the local library, cracked by a blown out window frame. Cracks in walls were documented in nearby Baturinsky and Kalachevo.

Electrophonic sounds were heard (SOM Sect. 1.6), but there was no evidence of an Electro Magnetic Pulse (EMP) under the track in neighboring Emanzhelinka. Due to shock wave induced vibrations, electricity and cell phone connectivity was briefly halted in Kunashak district at the far northern end of the damage area. Gas supply was briefly stopped in some districts due to valves reacting to the vibrations.

People who reported looking at the bright fireball found it painful, but glancing away prevented lasting eye damage. Of 1,113 respondents to an internet survey who were outside at the time, 25 were sunburned (2.2%), 315 felt hot (28%) and 415 (37%) warm (SOM Sect. 2.2). Mild sunburns were reported throughout the survey area (Table S7), reflecting the fact that UV flux density falls off slowly as $\sim r^{-2}$. In Korkino, 30 km from the point of peak brightness, one resident reported getting mild sunburn in the face, followed by losing skin flakes later. Such effects occur at a minimum erythema dose of ~1,000 J/m^2 (14) of 290-320 nm radiation (mostly UV-B). Assuming 6,000 K radiation (*9*), the calculated dose would have been ~200 J/m^2 at Korkino. Ground-reflectance of UV light by snow may have further increased the dose.

Out of the total 1,674 collected internet queries, 374 mention 452 injuries or inconveniences (SOM Sect. 2.2). Of those, 5.3% reported sunburn, 48% eyes hurt, and 2.9% felt retinal burns. Because of the shock wave, 6.4% had a concussion or were mentally confused, upset, or exhausted as a result of excessive stress. Flying glass and falling building debris affected a relatively small fraction of respondents: 4.8% had cuts and 2.9% had bruises, but no bones were broken.

The percentage of people asking for medical assistance (Table S10) dropped with distance according to $r^{-3.2\pm0.5}$ (SOM Sect. 2.1). The majority of injuries (1,210) took place in the densely populated Chelyabinsk city, but the highest fraction of people asking for assistance was near the trajectory in Korkinsky district (0.16%).

Meteorite Recovery

Shock radiation contributed to surface heating and ablation, but did not completely evaporate all fragments of Chelyabinsk, unlike in the case of Tunguska (*3*). Meteorites of ~ 0.1g fell near Aleksandrovka, masses of ~100g near Deputatskiy, and one of 3.4 kg further West near Timiryazevskiy. One meteorite hit the roof of a house in Deputatskiy (Fig. S46). Falling-sphere models suggest they originated at 37-29 km altitude (Fig. S52). The location of the meteorites is consistent with prevailing NW winds of 5-15 m/s (Fig. S24). An estimated 3,000-5,000 kg fell in this area (SOM Sect. 3.1).

Two main fragments survived the disruption at 29.7 km. They flared around 24 km, then one fell apart at 18.5 km, while the other remained luminous down to 13.6 km (Figs. 1 and S15). Lightcurve modeling (SOM Sect. 1.2) suggests that from this material another ~1 ton in larger

fragments up to 200-300 kg in mass reached the ground. A 7×8-m sized hole was discovered in 70-cm thick ice on Lake Chebarkul, in line with the trajectory (Fig. S53). Small meteorite fragments, many containing curved surfaces with fusion crust, were recovered over an area up to 50 m from the impact location (Fig. 4C). Impact models (Fig. S18, S54) confirm a 200-400 kg meteorite would be required to create such a hole. Recovery efforts of the main mass at the lake bed is still on going as of this writing.

The combined 4-6 t of surviving meteorites is only 0.03-0.05% of the initial mass. 76% of the meteoroid evaporated, with most of the remaining mass converted into dust (SOM Sect. 1.3). The Tunguska event, in contrast, left no recovered meteorites on the ground. Witnesses reported smelling "sulfur" and burning odors over a wide region concentrated near the fireball trajectory, starting about an hour after the fireball and lasting through much of the day (SOM Sect. 1.5, Fig. S34).

Characterization of Recovered Meteorites

The unusually effective fragmentation and small surviving mass may have been caused by structural and material weakness. The asteroid had a lower compressive strength than the ~330 MPa measured for recovered meteorites (Section S4.1). The lightcurve (Fig. 2) is modeled with fragmentation starting at a low 0.2 MPa dynamic pressure, but tolerating higher pressure with decreasing fragment size. This is similar to other impacts where initial weakness was attributed to macroscopic cracks or microscopic porosity (*15*). For Chelyabinsk, however, the physical weakness is not microporosity related. X-ray computed tomography (SOM Sect. 4.2) provided a degree of compaction consistent with the lack of intragranular porosity typical of LL chondrites (*16*).

Some laboratory broken meteorites fragmented along shock veins (Fig. S55), a possible weakness in the material that could have contributed to the abundant dust formation. The meteorite is composed of a breccia (*17*) of mildly-shocked lighter clasts and moderately-shocked darker clasts with abundant thin to cm-wide shock melt veins (Fig. 4A, SOM Sect. 4.4). A peculiar feature is that these shock veins show a metal layer located ~20 microns inside the vein, but follow the outer contours of the vein (Fig. 4B). This could contribute to weakness. Metal-rich tendrils also project outward from the vein.

The mineral compositional ranges (SOM Sect. 4.4) are slightly larger than those reported before *(18)*, but still compatible with a classification as LL5, shock stage S4 *(19)*. The classification as LL chondrite is substantiated by oxygen and chromium isotope studies (SOM Sect. 4.5-4.7), which put the meteorite near the L-end of the LL field *(20, 21)* (Figs. 4D, S68). Iron content and oxidation state also support the LL chondrite classification (Figs. 4E, Fig. S58). Rare Earth element abundances are more similar to L chondrites (Fig. 4F, Tab. S18), while one measured reflectance spectrum better matched that of H chondrites (Fig. S72), pointing to compositional heterogeneity.

The Chelyabinsk (LL) parent body experienced a significant thermal and/or collision resetting event 115±21 Ma after formation of the Solar System *(25),* not seen in most other LL ordinary chondrites, possibly due to a significant impact event near its site of origin on the parent body. The phosphate U-Pb age is 4,452 ± 21 Ma (SOM Sect. 4.8, Fig. S70), much younger than the majority of other ordinary chondrites phosphate ages dated by conventional TIMS methods *(22,23)*. Perhaps one other piece of evidence for this is the 4.48±0.12 Ga Pb-Pb isochron age of phosphates in a granite-like fragment found in a LL3-6 ordinary chondrite regolith breccia Adzhi-Bogdo (*24*), an observed fall in Mongolia in 1949.

Chelyabinsk has significant common orientation of metal grains indicating an extraordinary impact-related petrofabric in the analyzed sample (Fig. S59), stronger than those seen to date for ordinary chondrites of any shock stage *(26)* (Fig. S60). This petrofabric reflects the most recent extraterrestrial shock event experienced by the Chelyabinsk meteorite.

The magnetic susceptibility value is at the upper end of the range for LL type meteorites (*27*). However, detailed analysis of the remanent magnetization suggests that the shock event or the conditions of atmospheric entry led to significant resetting of the remanence (SOM Sect. 4.3).

The most recent heating events are normally recorded by thermoluminescence (TL) (SOM Sect. 4.10). The induced TL level is lower than other chondrite types 5 and 6, however, possibly because shock metamorphism to the level of S4 (30-35 GPa) (Fig. S79) destroyed feldspar, the mineral phase responsible for the thermoluminescence signal (*28*). Atmospheric heating did not cause loss of natural TL signal, the steep thermal gradient being consistent with a very thin fusion crust on the measured samples (*29*). The natural TL value is consistent with the asteroid being heated at a perihelion distance of 0.6-0.8 AU (Table 1).

The shock did not remove all organic matter in the meteorite. Methanol-soluble polar organic compounds (Sect. S4.11) were detected in impact melt vein and chondritic fractions using electrospray ionization ion cyclotron resonance Fourier-Transform mass spectrometry *(30)*. Out of more than 18,000 resolved mass peaks, 2,536 could be assigned to compounds containing C, H, N, O, S. The organic signature is typical of other shocked LL chondrites, showing a higher abundance of oxygen and nitrogen atoms in the impact melt. The presence of oxygenated sulfur is indicated by CHOS compounds containing on average 3 more oxygen atoms than CHO and CHNO compounds. The high abundance of CHOS compounds in homologous series across the entire mass range testifies that most of these did not result from contamination following the fall and subsequent handling.

Impact shock induced fracturing on the Chelyabinsk parent body was followed by melting of metal and sulfides, which are pressure-driven through the meteorite. There are cases were this increased a meteorite's mechanical strength, the residual heat facilitating the process. However, in the case of Chelyabinsk, the production of cracks weakened the meteorite more than shock melting increased its strength.

Source and Evolution of the Chelyabinsk Meteoroid

Chelyabinsk adds the first LL4-6 type meteorite with a pre-atmospheric orbit (SOM Sect. 1.1) to a short list of 18 other meteorite types for which pre-atmospheric orbits were derived from video or photographic records summarized in *(1)*. Only 8.2% of falls are LL chondrites *(31)*.

The meteorite is of particular interest because it is of the same type as asteroid Itokawa, from which samples were received in the Hayabusa mission *(32)*. Both have similar low-inclined low-semi-major axis orbits (Table 1), which, according to a previous model *(33),* imply a 62 %, 11%, and 25% probability for Chelyabinsk (and 71%, 0%, and 29% probability for Itokawa) of originating from the secular ν_6 resonance, the 3:1 mean-motion resonance, and the Intermediate Mars Crosser region, respectively. Multiplying these probabilities, assuming all LL chondrites enter the NEO region through the same escape route, there is now an 86% probability that they originated from ν_6. This supports the hypothesis *(34)* that they originated from the inner part of the LL-type *(35)* Flora asteroid family, which straddles the ν_6 resonance in 1.6-7.7º inclined orbits *(36)*.

As a group, LL chondrites have a cosmic ray exposure age peaking around ~17 My *(34)*. Chelyabinsk was exposed only since ~1.2 My (SOM Sect. 4.12). The responsible breakup that first exposed the Chelyabinsk meteoroid surface to cosmic rays was not likely part of the cascade of collisions in the asteroid main belt that followed the formation of the Flora family. Fast pathways exist that can bring meteoroids from all three resonances into a Chelyabinsk-like orbit in about 0.2 My (Table S6), but such cases are rare. Because of that, Chelyabinsk likely lost overburden since being ejected from the resonance, due to breakup from either thermal stresses, rotational spin-up, or from tidal forces in terrestrial planet encounters. The structural weakness may have come from macroscopic cracks or a weakly consolidated rubble pile morphology.

If tidal forces disrupted the Chelyabinsk meteoroid (*37*), events were set in motion 1.2 My ago during what was likely an earlier close encounter with Earth, when a 20-m sized chunk of sub-surface Flora-family parent body rubble, rich in shock veins, separated from a larger object. The rest of that rubble could still be part of the near-Earth object population.

References and Notes:

1. P. Jenniskens, M. D. Fries, Q.-Z. Yin, et al., Radar-enabled recovery of the Sutter's Mill meteorite, a Carbonaceous Chondrite Regolith Breccia. *Science* **338**, 1583-1587 (2012).
2. M. B. E. Boslough, D. A. Crawford, Shoemaker-Levy 9 and Plume-forming impacts on Earth. *Annals of the New York Academy of Sciences* **822**, 236-282 (1997).
3. V. V. Svetsov and V. V. Shuvalov, Tunguska catastrophe of 30 June 1908. In: Catastrophic events caused by cosmic objects, V. Adushkin, I. Nemtchinov (eds.), Springer, pp. 227-267 (2008).
4. D. R. Christie, P. Campus, The IMS infrasound network: Design and establishment of infrasound stations. In: *Infrasound Monitoring for Atmospheric Studies* (eds., A. Le Pichon, E. Blanc and A. Hauchecorne), Dordrecht: Springer, pp. 29–75 (2010).
5. D. Yeomans, P. Chodas, Additional Details on the Large Fireball Event over Russia on Feb. 15, 2013. *NASA NEO Program Office announcement* (March 1, 2013).
6. Materials and methods are available as supporting material on *Science Online*.
7. E. Tagliaferri, R. Spalding, C. Jacobs, S. P. Worden, A. Erlich, Detection of meteorite impacts by optical sensors in Earth orbit. In: Hazards due to comets and asteroids, Space Science Series, Tucson, University of Arizona Press, p. 199 (1994).

8. T. A. Ens, P. G. Brown, W. N. Edwards, E. A. Silber, Infrasound production of bolides: A global statistical study. *J. Atmosph. Solar Terr. Phys.* **80**, 208–209 (2012).
9. I. V. Nemtchinov, V. V. Svetsov, I. B. Kosarev, A. P. Golub', O. P. Popova, V. V. Shuvalov, R. E. Spalding, C. Jacobs, E. Tagliaferri, Assessment of Kinetic Energy of Meteoroids Detected by Satellites-Based Light Sensors. *Icarus* **130**, 259-274 (1997).
10. D. O. Revelle, Z. Ceplecha, Bolide physical theory with application to PN and EN fireballs. *ESA Special Publ.* **495**, 507-512 (2001).
11. J. Borovicka, P. Spurny, L. Shrbeny, Trajectory and orbit of the Chelyabinsk superbolide. CBET 3423, IAU Central Bureau for Astronomical Telegrams, D. W. E. Green (ed.), p. 1-1 (2013).
12. J. Zinn, J. Drummond, Observations of persistent Leonid meteor trails: 4. Buoyant model rise/vortex formation as mechanism for creation of parallel meteor train pairs. *JGR Space Physics* **110**, CiteID A04306 (2002).
13. S. Glasstone, P. J. Dolan, The effects of nuclear weapons. Third edition. U.S. Government Printing Office Washington, D.C., 1- 174 (1977).
14. M.-W. Huang, P.-Y. Lo, K.-S. Cheng, Objective assessment of sunburn and minimal erythema doses: Comparison of noninvasive in vitro measuring techniques after UVB irradiation. *EURASIP Journal on Advances in Signal Processing* 2010:483562. doi: 10.1155/2010/483562 (2010).
15. O. Popova, J. Borovicka, W. K. Hartmann, P. Spurny, E. Gnos, I. Nemtchinov, J. M. Trigo-Rodríguez, Very low strengths of interplanetary meteoroids and small asteroids. *Meteorit. Planet. Sci.* **46**, 1525–1550 (2011)
16. G. J. Consolmagno, D. T. Britt, R. J. Macke, The significance of meteorite density and porosity. *Chemie der Erde* **68**, 1–29 (2008).
17. A. Bischoff, E. R. D. Scott, K. Metzler, C. A. Goodrich, Nature and origins of meteoric breccias. In: *Meteorites and the Early Solar System II*, (eds, D. S. Lauretta, H. Y. McSween Jr.), University of Arizona Press, Tucson, AZ, pp. 679–712 (2006).
18. M. A. Nazarov, D. D. Badyukov, N. N. Kononkova, and I. V. Kubrakova, Chelyabinsk. Meteoritical Bulletin: Entry for Chelyabinsk: http://www.lpi.usra.edu/meteor/metbull.php?code=57165 (2013).

19. D. Stöffler, K. Keil, E. R. D. Scott, Schock metamorphism of ordinary chondrites. *Geochimica et Cosmochimica Acta* **55**, 3845–3867 (1991).

20. R. N. Clayton, T. K. Mayeda, J. N. Goswami, E. J. Olsen, Oxygen isotope studies of ordinary chondrites. *Geochim. Cosmochim. Acta* **55**, 2317–2337 (1991).

21. A. Trinquier, J.-L. Birck, C. J. Allègre. Widespread ^{54}Cr Heterogeneity in the Inner Solar System. *Astrophy. J.* **655**, 1179-1185 (2007).

22. C. Göpel, G. Manhès, C. J. Allègre, U-Pb systematics of phosphates from equilibrated ordinary chondrites. *Earth and Planetary Science Letters* **121**, 153-171 (1994).

23. Y. Amelin, Meteorite phosphates show constant ^{176}Lu decay rate since 4557 million years ago. *Science* **310**, 839-841 (2005).

24. K. Terada, A. Bischoff, Asteroidal granite-like magmatism 4.53 Gyr ago. *Astrophys. J. Lett*. **699**, L68–L71 (2009).

25. J. N. Connelly, M. Bizzarro, A. N. Krot, Åke Nordlund, D. Wielandt, M. A. Ivanova, The absolute chronology and thermal processing of solids in the solar protoplanetary disk. *Science* **338**, 651-655 (2012).

26. J. M. Friedrich, J. C. Bridges, M.-S. Wang, M. E. Lipschutz, Chemical studies of L chondrites. VI: Variations with petrographic type and shock-loading among equilibrated falls. *Geochimica et Cosmochimica Acta* **68,** 2889-2904 (2004).

27. J. Gattacceca, P. Rochette, Toward a robust normalized magnetic paleointensity method applied to meteorites. *Earth Planet. Sci. Lett*. **227**, 377–393 (2004).

28. C. P. Hartmetz, D. W. G. Sears, Thermoluminescence properties of shocked and annealed plagioclases with implications for meteorites. *Meteoritics* **22**, 400-401 (1988).

29. D. W. Sears, A. A. Mills, Temperature gradients and atmospheric ablation rates for the Barwell meteorite. *Nature Physical Science* **242**, 25-26 (1973).

30. N. Hertkorn, M. Frommberger, M. Witt, B. P. Koch, P. Schmitt-Kopplin, E. M. Perdue, Natural Organic Matter and the Event Horizon of Mass Spectrometry. *Analytical Chemistry* **80**, 8908-8919 (2008).

31. T. L. Dunn, T. H. Burbine, W. F. Bottke, J. P. Clark, Mineralogies and source regions of near Earth asteroids. *Icarus* **222**, 273-282 (2013).

32. T. Nakamura, T. Noguchi, M. Tanaka, M. E. Zolensky, M. Kimura, A. Tsuchiyama, A. Nakato, T. Ogami, H. Ishida, M. Uesugi, T. Yada, K. Shirai, A. Fujimura, R. Okazaki, S. A.

Sandford, Y. Ishibashi, M. Abe, T. Okada, M. Ueno, T. Mukai, M. Yoshikawa, and J. Kawaguchi, Itokawa dust particles: A direct link between S-type asteroids and ordinary chondrites. *Science* **333**, 1113-1116 (2011).

33. W. F. Bottke, A. Morbidelli, R. Jedicke, J.-M. Petit, H. F. Levison, P. Michel, T. S. Metcalfe, De-biased orbital and absolute magnitude distributions of Near Earth Objects. *Icarus* **156**, 339-433 (2000).
34. P. Michel, M. Yoshikawa, Dynamical origin of the asteroid (25143) Itokawa: the target of the sample-return Hayabusa space mission. *Astron. Astrophys.* **449**, 817-820 (2006).
35. V. Reddy, J. M. Carvano, D. Lazzaro, T. A. Michtchenko, M. J. Gaffey, M. S. Kelley, T. Mothé-Diniz, A. Alvarez-Candal, N. A. Moskovitz, E. A. Cloutis, E. L. Ryan, Mineralogical characterization of Baptistina Asteroid Family: Implications for K/T impactor source. *Icarus* **216**, 184-197 (2011).
36. D. Nesvorny, A. Morbidelli, D. Vokrouhlicky, W. F. Bottke, M. Broz, The Flora family: A case of the dynamically dispersed collisional swarm? *Icarus* **157**, 155-172 (2002).
37. E. Schunová, M. Granvik, R. Jedicke, G. Gronchi, R. Wainscoat, S. Abe, Searching for the first near-Earth object family. *Icarus* **220**, 1050-1063 (2012).
38. W. F. McDonough, Compositional model for the Earth's core. In: *The Mantle and Core, Vol. 2. Treatise on Geochemistry*, R. W. Carlson (ed.), Elsevier-Pergamon, Oxford, 547–568 (2003).
39. J. T. Wasson, G. W. Kallemeyn, Compositions of chondrites. *Phil. Trans. Roy. Soc. London A* **325**, 535–544 (1988).
40. J. Troiano, D. Rumble III, M. L. Rivers, J. M. Friedrich, Compositions of three low-FeO ordinary chondrites: indications of a common origin with the H chondrites. *Geochimica et Cosmochimica Acta* **75**, 6511-6519 (2011).
41. J. M. Friedrich, M.-S. Wang, M. E. Lipschutz, Chemical studies of L chondrites. V: Compositional patterns for 49 trace elements in 14 L4-6 and 7 LL4-6 Falls. *Geochimica et Cosmochimica Acta* **67**, 2467-2479 (2003).

Acknowledgments: The Russian Academy of Sciences field study of the Chelyabinsk airburst was supported by the Institute for Dynamics of Geospheres and grants of the Federal Targeted Program "Scientific and Educational Human Resources of Innovation-Driven Russia" and the RAS Presidium Program "Fundamental Problems of Investigation and Exploration of the Solar System". The office of Chelyabinsk Oblast Governor Mikhail Yurevich provided assistance. Sergey Petukhov and Igor Talyukin from the Universe History Museum in Dedovsk contributed samples, as did Mark Boslough of Sandia National Laboratories. Ulrich Johann (Astrium Satellites GmbH) calculated the Chebarkul hole position from Pléiades 1A satellite observations. David F. Blake provided use of a petrographic microscope. PJ acknowledges support from the NASA Near Earth Object Observation Program, QZY and MZ from the NASA Cosmochemistry Program.

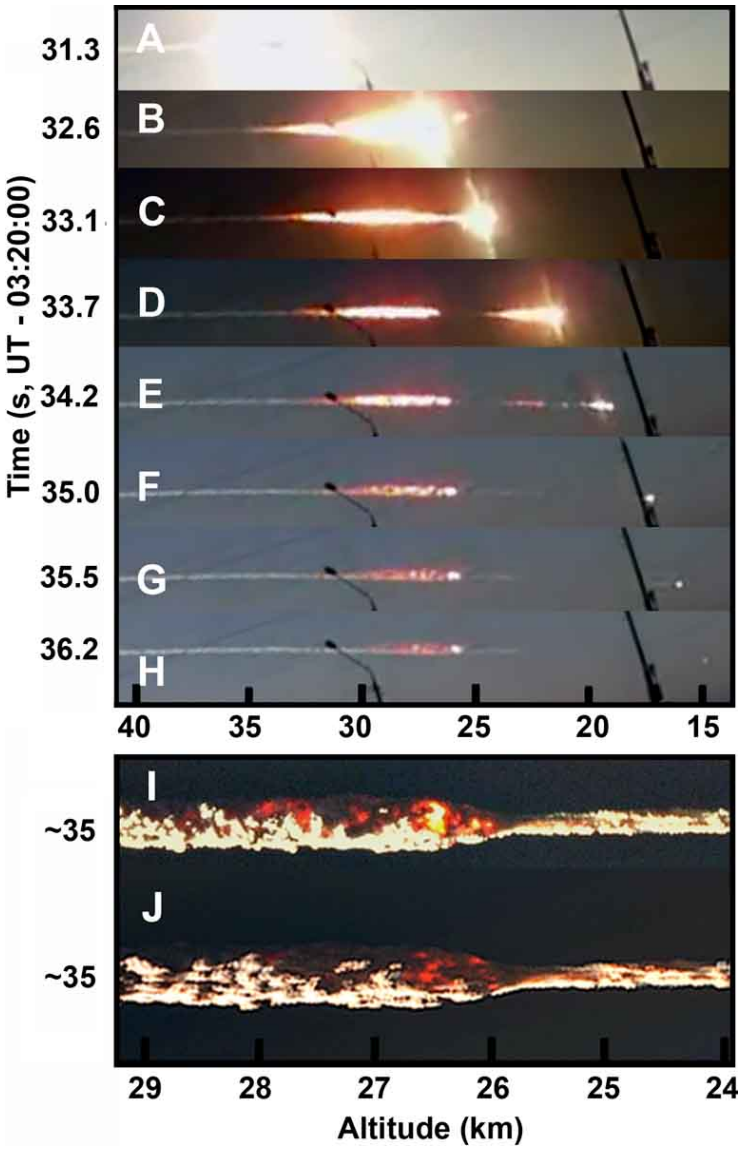

Fig. 1. Meteoroid fragmentation stages in video taken by Alexander Ivanov in Kamensk-Uralskiy. **(A)** Fireball just before peak brightness, at moment when camera gain first adjusted. **(B)** End of main disruption. **(C)** Onset of secondary disruption. **(D)** End of secondary disruption, main debris cloud continues to move down. **(E)** Two main fragments remain. **(F)** Single fragment remains. **(G)** Thermally emitting debris cloud at rest with atmosphere. **(H)** Final fragment continues to penetrate. Meteor moved behind distant lamp posts. **(I-J)** Detail of the thermal emission from a photograph by Mr. Dudarev **(I)** and Marat Ahmatvaleev **(J)**, after sky subtraction with high-pass filter and contrast enhancement. Altitude scale is uncertain by ±0.7 km.

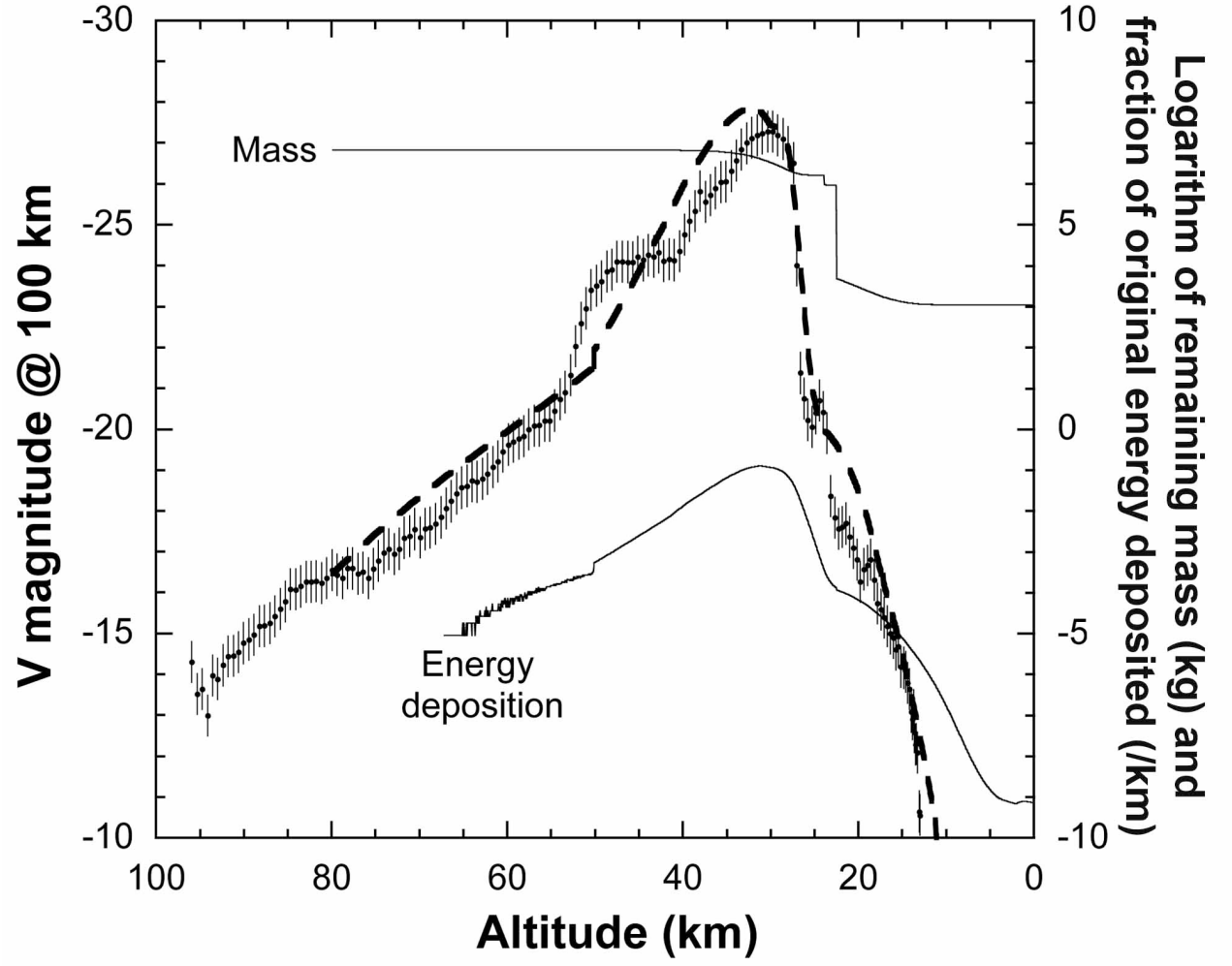

Fig. 2. Fireball visual magnitude irradiance lightcurve, normalized to 100 km distance. The bold dashed line shows the model fit to the lightcurve (SOM Sect. 1.2), with thin lines showing total mass of all fragments passing a given altitude (kg) and the altitude dependent rate of energy deposition as a fraction of the original kinetic energy (km^{-1}).

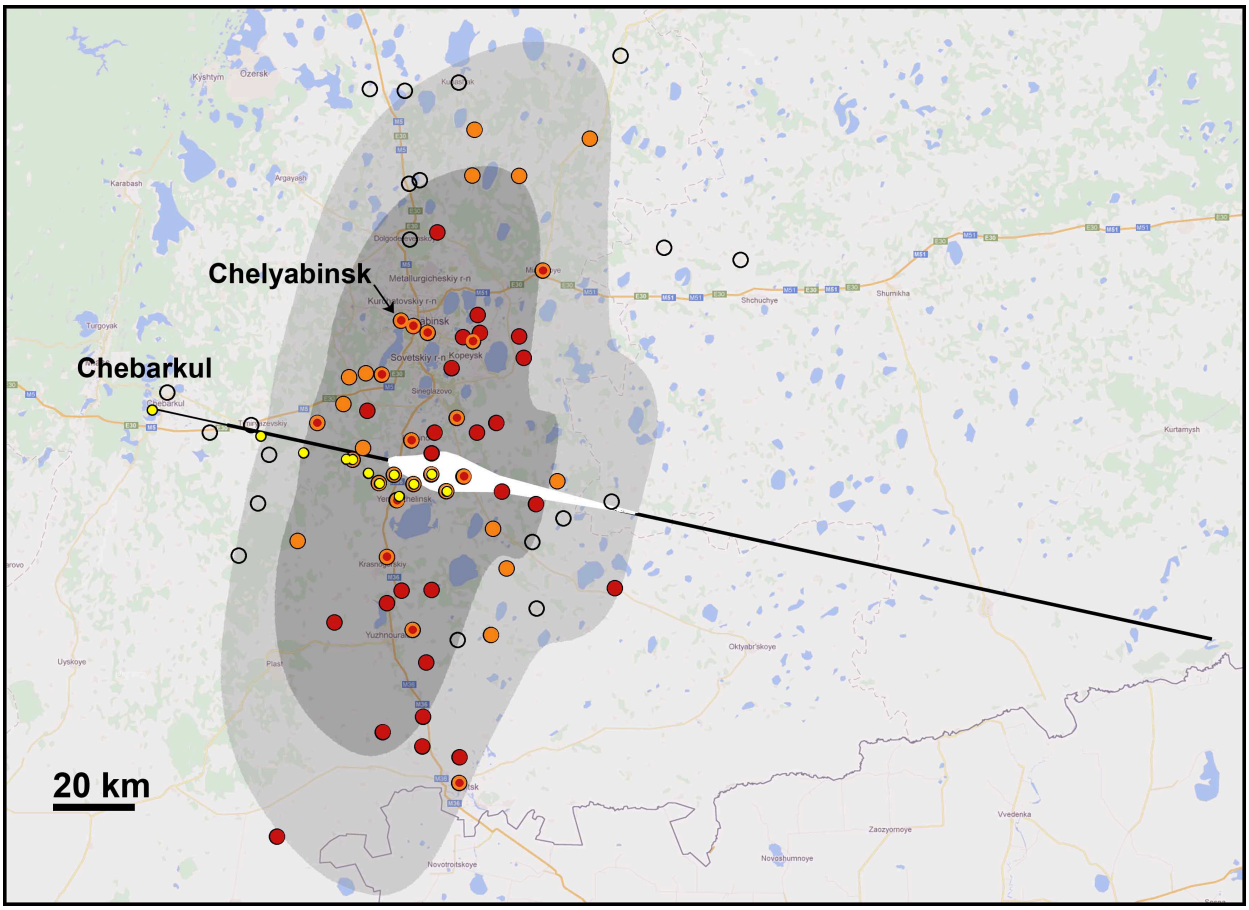

Fig. 3. **Model of overpressure on the ground** (dark Δp > 1,000 Pa, light Δp > 500 Pa) on top of a map of sites with glass damage, each point represents one of many villages or city districts scattered throughout the area. Field survey data are shown in solid orange circles for reported damage and open black circles for no damage, while data from government reports are shown in solid red circles. Also shown are the location of meteorite finds (yellow points) and the ground-projected fireball trajectory, moving from 97 km altitude right to 14 km altitude left (black line, with white showing peak radiation).

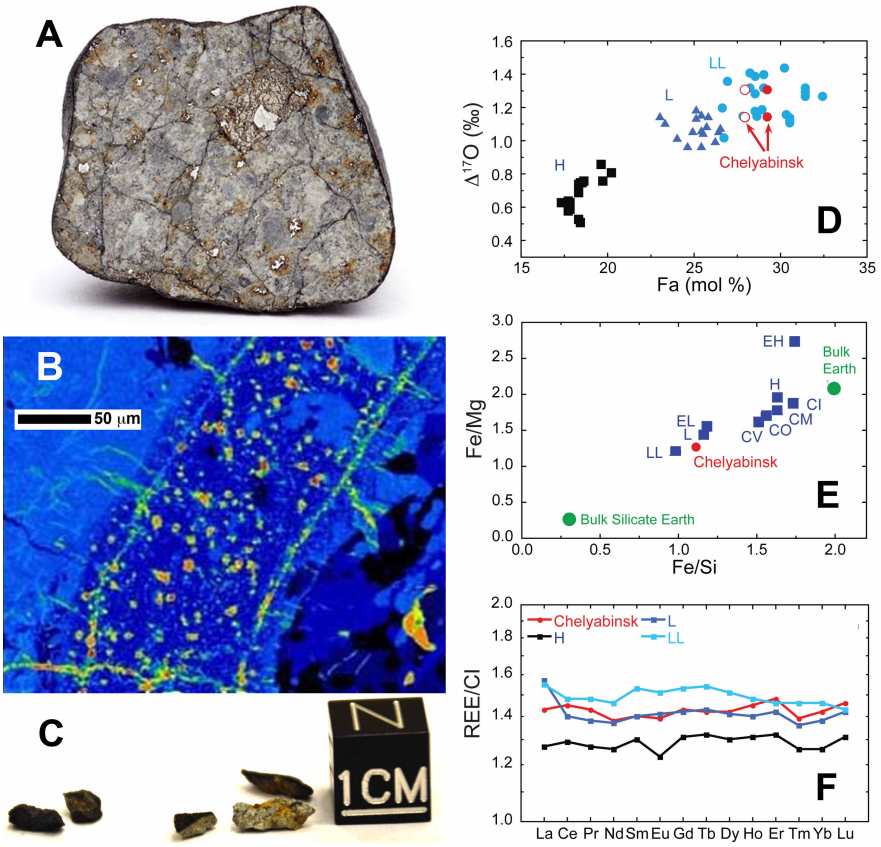

Fig. 4. Meteorite material properties, chemical and isotopic compositions. (A) Chelyabinsk meteorite (diameter ~4 cm) showing shock veins. **(B)** Fe element map of a shock vein. Note the metal layer (shown in green) located ~20 microns inside the vein. **(C)** Meteorite fragments recovered from the ice covered lake Chebarkul. **(D)** $\Delta^{17}O$ vs. Fa mol% of olivine in Chelyabinsk, compared to other ordinary chondrites of type H, L, and LL *(36)*. Fa is defined as mole ratio of Fe/(Fe+Mg) in olivine. Average $\Delta^{17}O$ values from UNM (1.15±0.06‰) and from KOPRI (1.31 ± 0.04‰) for Chelyabinsk likely reflect indigenous heterogeneity in oxygen isotopes. Solid symbols are Fa number measured in this study (SOM Sect. S4.3), while open symbols are from *(18)*. **(E)** Ratio plots of the three major elements (Mg, Si, Fe; together with oxygen >90% of mass) for Chelyabinsk and the main chondrite groups. The bulk Earth and bulk silicate Earth compositions were taken from *(38)*, chondrite compositions from *(39)*. **(F)** CI chondrite normalized rare earth elemental pattern of Chelyabinsk compared to the average chondrite group compositions of *(40,41)*.

Table 1. Atmospheric trajectory and pre-atmospheric orbit for the Chelyabinsk meteoroid, with 2 standard deviation uncertainties. Angular elements are for equinox J2000.0.

Atmospheric trajectory:	Chelyabinsk	Preatmospheric orbit:	Chelyabinsk	Itokawa
H_b (beginning height - km)	97.1±1.6	T_J (Tisserand's parameter)	3.87±0.24	4.90
H_m (peak brightness - km)	29.7±1.4	a (semimajor axis - AU)	1.76±0.16	1.324
H_f (disruption - km)	27.0±1.4	e (eccentricity)	0.581±0.018	0.280
H_e (end height - km)	13.6±1.4	q (perihelion distance - AU)	0.739±0.020	0.953
V_∞ (entry speed - km/s)	19.16 ± 0.30	ω (argument of perihelion - º)	108.3±3.8	162.8
h (entry elevation angle - º)	18.3 ± 0.4	Ω (longitude of ascending node - º)	326.4422±0.0028	69.1
a_z (entry azimuth angle from South - º)	283.2±0.4	i (inclination - º)	4.93±0.48	1.6
V_g (geocentric entry speed – km/s)	15.3±0.4	Q (aphelion distance - AU)	2.78±0.20	1.70
Ra_g (geocentric right ascension of radiant - º)	333.2±1.6	T_p (perihelion time)	2012-12-31.9±2.0	2013-07-10.8
Dec_g (geocentric declination of radiant - º)	+0.3±1.8	Epoch (ET)	2013-02-15.139	2013-04-18.0

Supplementary Materials:

www.sciencemag.org

Asteroid Orbit and Atmospheric Entry
Damage Assessment
Meteorite Recovery
Meteorite Characterization
Figures S1-S87
Tables S1-S24
References (*42-163*)